The Stress-Relief Cracking Susceptibility of a New Ferritic Steel — Part 2: Multiple-Pass Heat-Affected Zone Simulations

The effect of using a multiple-pass weld procedure on the stress-relief cracking susceptibility of a new ferritic steel was investigated and compared to single-pass samples

BY J. G. NAWROCKI, J. N. DUPONT, C. V. ROBINO AND A. R. MARDER

ABSTRACT. The stress-relief cracking susceptibility of multiple-pass welds in HCM2S, a new ferritic steel, and standard 2.25Cr-1Mo steel has been evaluated and compared to single-pass weld results using Gleeble techniques. Simulated coarse-grained heat-affected zones (CGHAZ) were produced using two- and three-pass thermal cycle simulations and tested at various postweld heat treatment (PWHT) temperatures. Light optical and scanning electron microscopy were used to characterize the CGHAZ microstructures. The multipass samples of each material failed along grain boundaries (prior austenite or packet) normal to the tensile axis and exhibited extensive plastic deformation, indicating that stress-relief cracking was avoided with the use of multipass simulations. The times to failure, when considering CGHAZ simulations, were longer than those of the single-pass samples at each PWHT temperature. The ductility increased with increasing PWHT temperature for each alloy and increased relative to the single-pass samples at each PWHT temperature. The differences in stress-relief cracking response between the single- and multiple-pass samples are discussed in terms of the microstructural changes that take place during the multiple-pass procedure and subsequent PWHT.

Introduction

In Part 1 of this investigation (Ref. 1), a range of single-pass weld thermal simulations and postweld heat treatment schedules were imposed on a new ferritic steel HCM2S and 2.25Cr-1Mo steel. HCM2S was shown to be more susceptible to stress-relief cracking than 2.25Cr-1Mo steel. Both alloys failed along prior austenite grain boundaries, but 2.25Cr-1Mo steel exhibited significant macroductility when tested at 325 MPa, whereas HCM2S exhibited little ductility. Lowering the applied stress in the 2.25Cr-1Mo steel samples to normalize for the yield strength resulted in lower ductility values from the stress-relief cracking tests.

Stress-relief cracking typically occurs due to a combination of precipitation strengthening of the grain interiors, a precipitate-free denuded zone, and/or temper embrittlement of the prior austenite grain boundaries (Ref. 2). In single-pass welds, stress-relief cracking mainly occurs in the CGHAZ region. However, with the exception of thin sections, welding Cr-Mo steels will require a multiple-pass procedure. Alloy steel weldments such as 2.25Cr-1Mo used for pressure vessels typically require a postweld heat treatment. This is done to relieve residual stresses, improve mechanical properties, and reduce hydrogen-cracking susceptibility of the HAZ. It is very difficult to PWHT large components after in-service repairs are performed. Multipass welding procedures or temper-bead techniques can be used to improve the toughness of the HAZ much like a PWHT. With this approach, the heat of subsequent passes acts to temper previous passes (Ref. 3). The prior austenite grain size can also be refined if the material is heated into the austenite region to a temperature lower than that reached during the first pass and recrystallization occurs. The reduced prior austenite grain size reduces hardenability and, for a given amount of segregant elements, provides more grain boundary area over which the segregants can be distributed. The result is with the formation of smaller prior austenite grains during multipass welding, the original CGHAZ may now have a microstructure that is more resistant to stress-relief cracking than the CGHAZ produced from a single-pass weld. The use of multipass or temper bead procedures can reduce the need for expensive, time-consuming PWHT operations. However, the weldments will be subjected to in-service temperatures ranging from approximately 500 to 700°C, and, therefore, the effect of elevated temperatures needs to be assessed. Also, for the temper bead procedure to be effective and reliable, there must be precise control of the bead size, sequencing and interpass temperature. Therefore, the objective of Part 2 of this research is to determine the effect of using a multiple-pass weld procedure on the stress-relief cracking susceptibility of 2.25Cr-1Mo and HCM2S alloys relative to single-pass welds.

KEY WORDS

Stress Relief
Multipass Welds
Cracking Susceptibility
PWHT
CGHAZ
Heat-Affected Zone
Temper Bead
Ferritic Steel

Experimental Procedure

Multipass Stress-Relief Cracking Tests

The compositions of 2.25Cr-1Mo and HCM2S alloys used in this research can be found in Part 1 (Ref. 1). Stress-relief cracking tests were performed using a Gleeble thermomechanical simulator.

J. G. NAWROCKI, J. N. DUPONT and A. R. MARDER are with Department of Materials Science and Engineering, Lehigh University, Bethlehem, Pa. C. V. ROBINO is with Materials Joining Department, Sandia National Laboratories, Albuquerque, N.Mex.

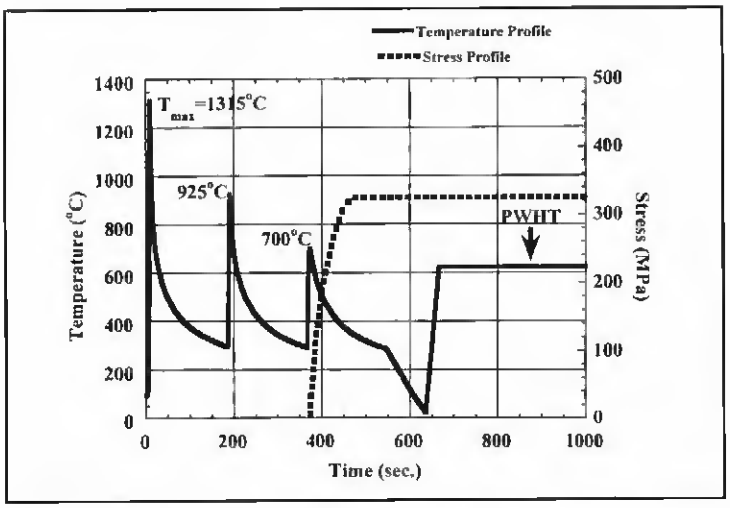

Fig. 1 — Schematic illustration of a three-pass weld simulation and stress-relief cracking test.

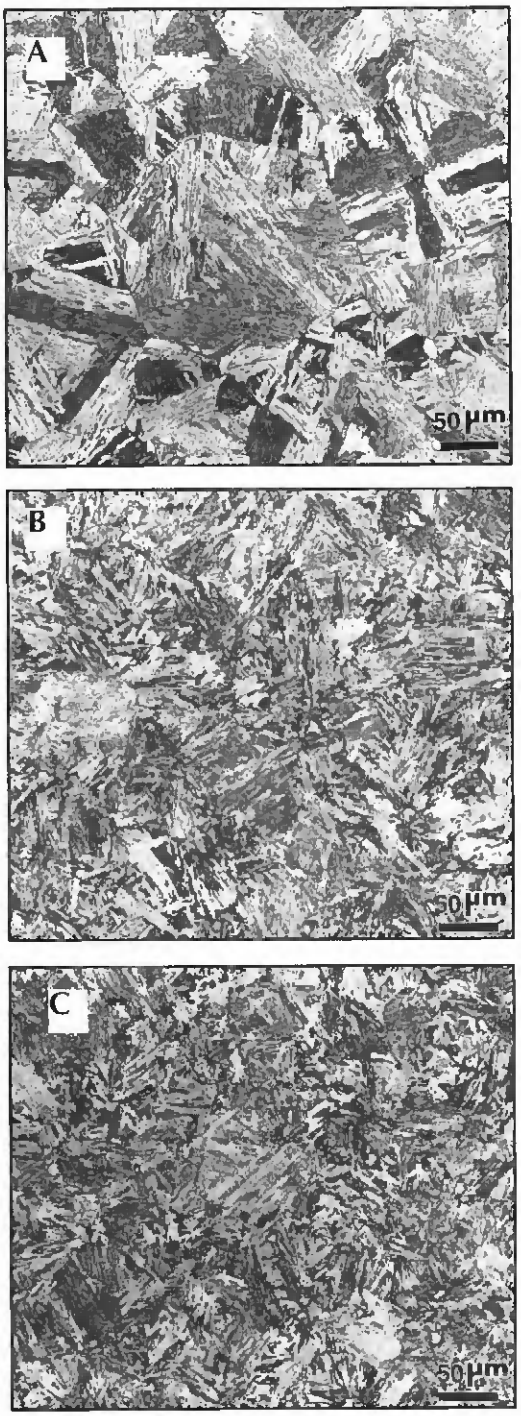

Fig. 2 — Photomicrographs of the CGHAZ. Heat-affected zone simulations of HCM2S. A — One pass; B — two passes; C — three passes.

Unnotched, cylindrical specimens (105 mm long, 10 mm in diameter) with threaded ends were used. A schematic illustration of a three-pass, stress-relief cracking test cycle can be seen in Fig. 1. Each thermal cycle was produced using an energy input of 2 kJ/mm and a preheat temperature of 93°C. The peak temperatures used for the first, second and third passes were 1315, 925, and 700°C, respectively. The interpass temperature was approximately 300°C. These thermal cycles are based on experimentally measured values from actual shielded metal arc welds (Refs. 4, 5). A temperature of 1315°C is representative of the peak temperature of the material adjacent to the fusion zone during welding. A temperature of 925°C is above the upper critical temperature, A_3, and the prior austenite grain size will be decreased relative to the first pass. The peak temperature of the third pass, 700°C, is sub-critical (below the A_1 temperature) and the material will not retransform to austenite upon heating. The third pass then acts as a tempering pass. A tensile stress was imposed on the sample during cooling of the last pass and held for the duration of the test to simulate the residual stresses present in an actual weldment. After cooling to room temperature, the samples were then subjected to a programmed, postweld heat treatment temperature and held at constant stress and temperature until failure. Postweld heat treatment (PWHT) temperatures ranged between 625 and 725°C. HCM2S was tested at a stress of 325 MPa and 2.25Cr-1Mo steel at 270 MPa. A lower stress was used for 2.25Cr-1Mo steel to help normalize the difference in yield strength between the two materials. HCM2S was tested using both two- and three-pass simulations, but 2.25Cr-1Mo steel was only tested using a two-pass simulation. Tests were performed under a vacuum of approximately 100 millitorr to prevent decarburization and oxidation of the samples, as well as decoherence of the thermocouples. The time to failure was recorded as the time elapsed after the PWHT temperature was reached until sample rupture. The ductility was measured as the reduction in area during PWHT.

One half of each fractured sample was reserved for fractographic examination by scanning electron microscopy. The remaining half was electroless Ni-coated to provide edge retention of the fracture surface. Longitudinal cross-sectional samples were then polished to a 0.04-µm finish using colloidal silica. Microhardness traces were performed on samples in the as-welded condition using a Knoop indenter and a 500-g load. Samples were etched using Vilella's reagent. Selected samples were also etched using a solution of 15 g sodium meta-bisulfite and 100 mL H_2O to reveal the prior austenite grain boundaries in the multipass samples.

Results

Typical as-welded CGHAZ microstructures of both single- and multiple-pass samples for HCM2S and 2.25Cr-1Mo alloys are shown in Figs. 2 and 3. The prior austenite grain size and subsequent packet size have been refined relative to the single-pass CGHAZs (Ref. 1). The prior austenite grain size of the multipass samples was ~43 µm compared to ~50 µm in the single-pass samples. However, the prior austenite grain boundaries were difficult to reveal in the multipass samples and the measurements represent approximate values and more error may be involved than in the single-pass samples. It can be seen from Figs. 2 and 3, however, that the average length of the laths in the single-pass samples is greater

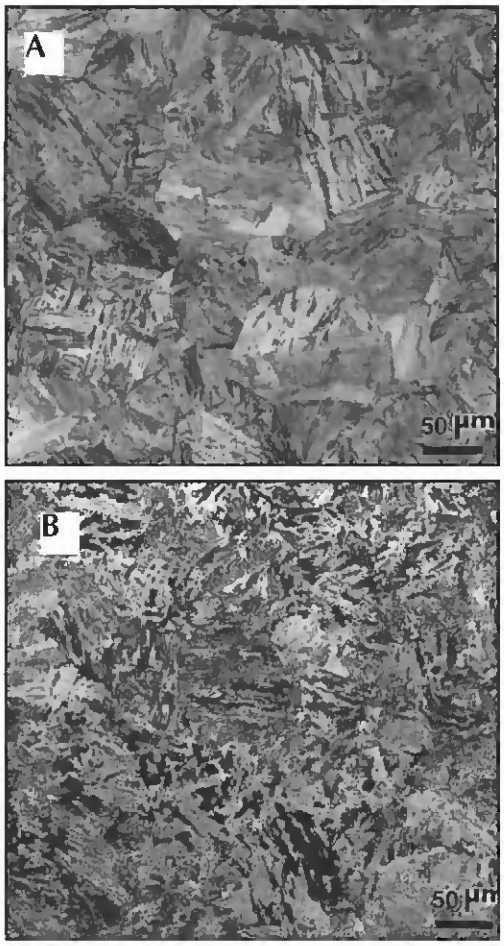

Fig. 3 — Photomicrographs of the CGHAZ. Heat-affected zone simulations of 2.25Cr-1Mo steel. A — One pass; B — two passes.

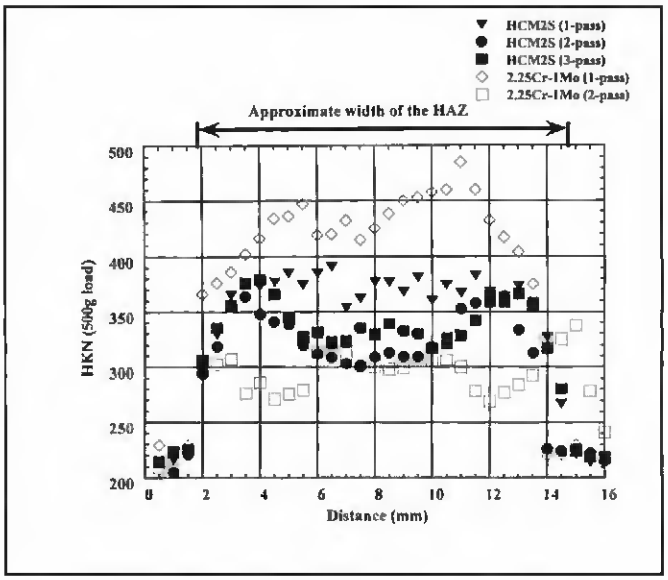

Fig. 4 — Hardness traverses across the HAZ of single- and multiple-pass simulation samples of HCM2S and 2.25Cr-1Mo steel.

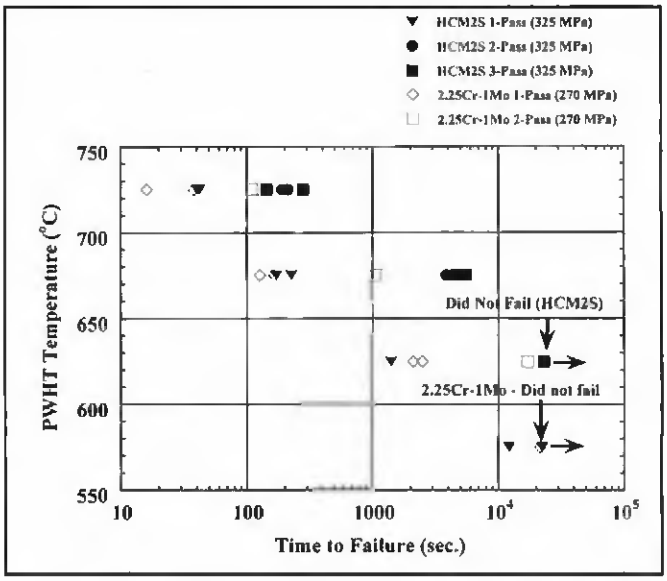

Fig. 5 — Postweld heat treatment temperature vs. the time to failure for single- and multipass HAZ simulation samples of HCM2S and 2.25Cr-1Mo steel.

than the multipass samples, which also indicates a larger apparent prior austenite grain size in the single-pass samples. The apparent limited amount of grain refinement in the multipass samples is due to the fast heating and cooling rates, and, therefore, the limited amount of time available for the transformation to austenite upon heating.

Figure 4 shows hardness traverses from each alloy in the multipass conditions relative to the single-pass hardness (2 kJ/mm energy input also). In the case of HCM2S alloy, the peak hardness dropped from a maximum of ~380 HKN in the single-pass sample to less than 350 HKN in the multiple-pass welds even though the prior austenite grain and packet size are smaller. The peak hardness of the 2.25Cr-1Mo alloy experienced a significant decrease in hardness from the first (~475) to the second pass sample (< 350).

Figure 5 is a plot of the PWHT temperature vs. the time to failure for both alloys from stress-relief cracking tests of single- and multiple-pass samples. Failure occurred in the former CGHAZ in every sample. The time to failure decreased as the PWHT temperature increased for each sample. This is mainly due to the decrease in yield strength with increasing temperature and does not mean the susceptibility to stress-relief cracking increases as the PWHT temperature increases. At each of the PWHT temperatures, the time to failure increased in the multiple-pass specimens relative to the single-pass samples for both alloys. In the case of HCM2S tested at 625°C, the multiple-pass specimen did not fail after over six hours and the test was stopped. This is approximately the time to failure for the single-pass samples at 575°C, which further emphasizes the increase in rupture life as a result of the multiple-pass procedure. For HCM2S, there was no discernable differences between the two- and three-pass samples. In the case of the 2.25Cr-1Mo alloy, failure did occur at 625°C, but the time to failure greatly increased relative to the single-pass samples. It should be noted that the single-pass 2.25Cr-1Mo samples tested at 575°C did not fail after six hours, and, therefore, multipass samples were not tested at this temperature.

Figure 6 shows the variation in reduction in area with PWHT for single- and multiple-pass weld samples of each alloy. In general for the 2.25Cr-1Mo steel, the

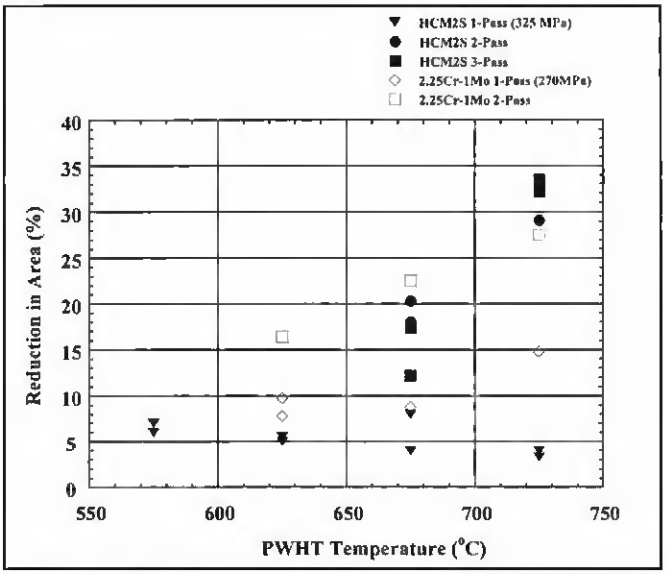

Fig. 6 — Reduction in area as a function of PWHT temperature for single- and multiple-pass HAZ simulation samples of HCM2S and 2.25Cr-1Mo steel.

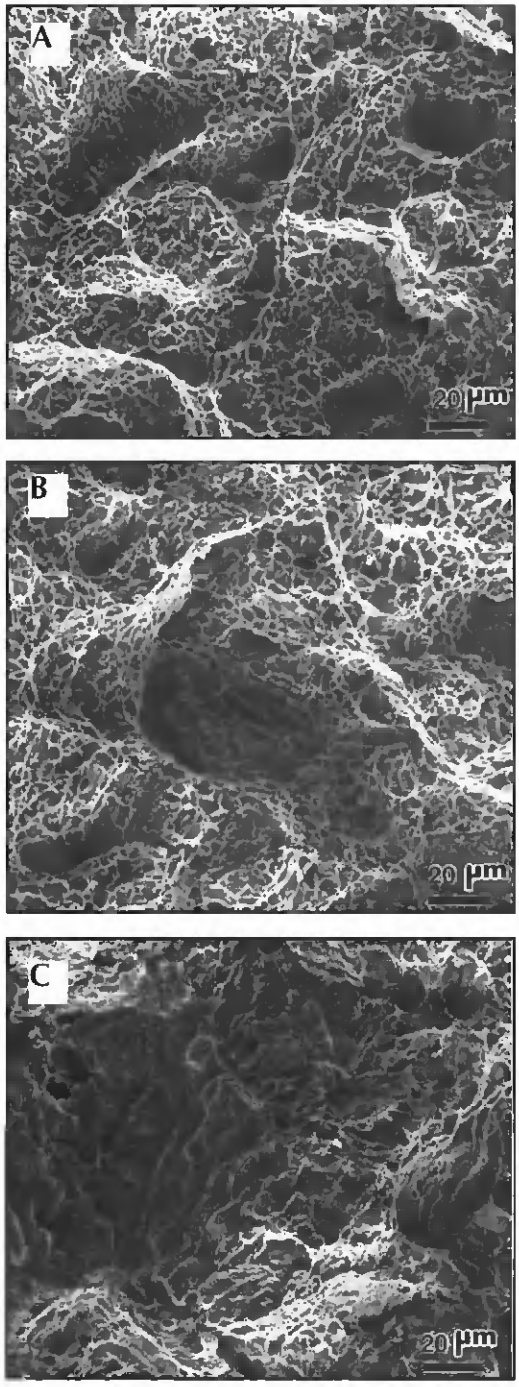

Fig. 7 — SEM photomicrographs of fracture surfaces of failed samples at 675°C. A — Two-pass HCM2S; B — three-pass HCM2S; C — two-pass 2.25Cr-1Mo steel.

ductility increased with increasing PWHT temperature. The reduction in area increased significantly in the two-pass samples relative to the single-pass samples at each PWHT temperature. The ductility is also shown to increase in the HCM2S alloy from the single-pass to the multipass weld samples. The PWHT temperature had no effect on the ductility of the single-pass samples of HCM2S. However, as the PWHT increased, the ductility increased for the multiple-pass specimens of HCM2S. There is no discernable difference between the results of the two- and three-pass samples.

Figure 7 shows SEM photomicrographs of the fracture surfaces of multiple-pass samples tested at a PWHT temperature of 675°C. Both the two- and three-pass HCM2S samples (Fig. 7A, B) exhibit extensive microvoid coalescence indicative of the high ductility values shown in Fig. 6. The 2.25Cr-1Mo two-pass sample (Fig. 7C) was shown to have similar ductility to the multiple-pass HCM2S samples in Fig. 6. Figures 8 and 9 show typical cross-sectional light optical photomicrographs acquired from fractured samples corresponding to those in Fig. 7. The white outer layer in Figs. 8A, 8C and 9A is an electroless Ni-coating. For the HCM2S alloy (Fig. 8A–E), it is now seen that failure occurred both intergranularly and transgranularly, which was not evident from observation of the fracture surfaces. Many secondary cracks can be seen behind the fracture surface with each being approximately normal to the direction of the applied tensile stress. The cracks are wavy as opposed to the sharp cracks found along prior austenite grain boundaries in the single-pass samples (Ref. 1). The cracks appear to run both across and along prior austenite grain and/or packet boundaries. The formation of voids is evident at both prior austenite grain boundaries (large arrow) and within prior austenite grains (small arrow) in Fig. 8E. Many small precipitates can be seen with a higher density located at prior austenite grain boundaries. Some carbides can also be seen within grain interiors. Carbides are known to act as microvoid nucleation sites in metallic materials during creep (Ref. 6) and conventional ductile failure (Refs. 7, 8).

In the case of the 2.25Cr-1Mo steel, failure also occurred predominantly along grain boundaries — Fig. 9. The cracks are wavy and irregular in contrast to the straight and sharp cracks found in the single-pass samples (Ref. 1). Figure 9C clearly shows the coalescence of voids along grain boundaries only in areas approximately normal to the applied tensile stress. Many carbides can be seen in the multiple-pass samples of 2.25Cr-1Mo alloy and previous work (Ref. 9) has shown that Fe-, Cr- and Mo-based carbides precipitate in this alloy under the processing conditions/heat treatments used in this research.

Discussion

The stress-relief cracking susceptibility of alloys can be determined by the combination of two criteria: ductility and mode of failure. As mentioned in Part 1 of this work (Ref. 1), ductility is often used to compare alloys when Gleeble simulation techniques are used (Refs. 10, 11). Alloys that can appreciably soften during PWHT

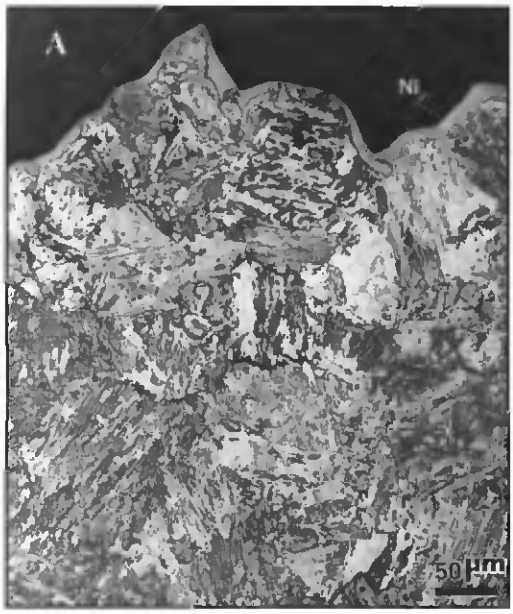

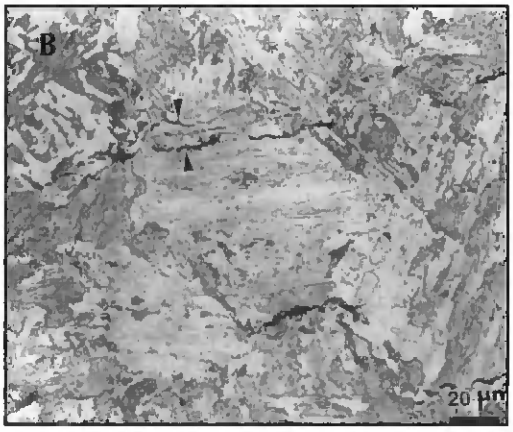

Tensile Axis

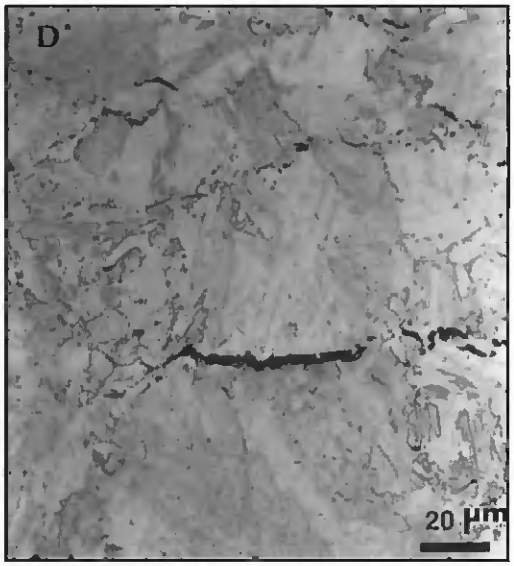

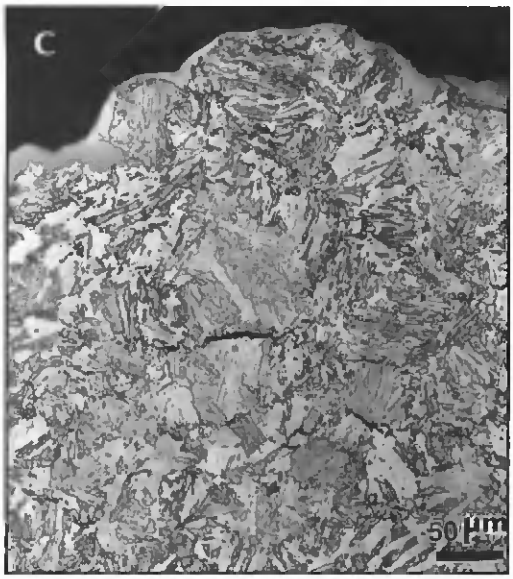

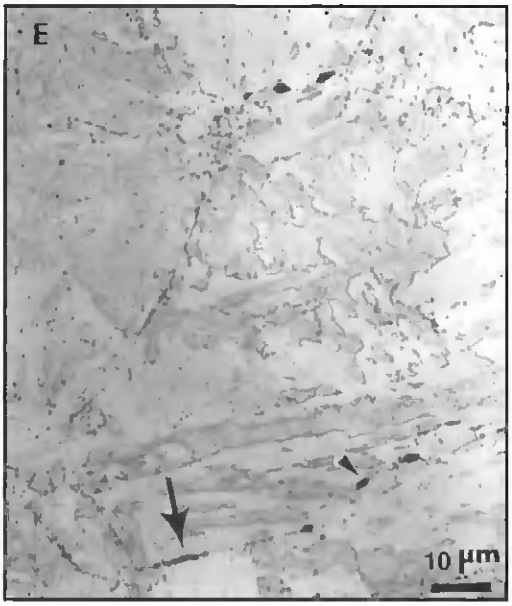

Tensile Axis

Fig. 8 — Photomicrographs of cross sections of HCM2S samples tested at 675°C. A, B — Two passes; C, D, E — three passes.

can relieve residual stresses by macroscopic yielding. Alloys that retain their strength through precipitation hardening and form a denuded zone adjacent to prior austenite grain boundaries are susceptible to low-ductility intergranular fracture typical of stress-relief cracking. When exposed to elevated temperatures during PWHT or in service, segregation of tramp elements to prior austenite grain boundaries can exacerbate stress-relief cracking. According to the criteria for stress-relief cracking susceptibility outlined by Vinckier and Pense (Ref. 10) as discussed in Part 1, the multiple-pass samples from both alloys evaluated in this study can generally he considered not susceptible to stress-relief cracking at each PWHT temperature. The HCM2S three-pass sample tested at 675°C is the only sample considered even slightly susceptible. It is interesting to note that the prior austenite grain size and resultant packet size decreased in the multipass weld samples relative to the single-pass samples. A decrease in prior austenite grain size alone should increase the strength and hardness (Refs. 12, 13). However, the hardness was shown to decrease in the finer-prior austenite-grained multipass samples relative to the larger prior austenite-grained single-pass samples. Any undissolved carbides present after the first pass may have coarsened or carbides may have formed during cooling after the transformation to martensite, *i.e.*, autotempering. This is especially true in materials having low carbon contents and, consequently, a high martensite start temperature such as HCM2S. In either case, the carbides will coarsen during subsequent passes, effectively lowering the hardness. If carbides formed during cooling (autotempering), these carbides will most likely be cementite. The secondary hardening phenomena occurs when more stable alloy carbides effectively replace the cementite particles. Due to the limited grain refinement after the second pass, the second and third passes may have acted as tempering passes during which time any carbides present will coarsen. Coarse particles are more difficult to dissolve and replace than small particles. Therefore, the coarse carbides present after the multipass procedure tend to retard any secondary hardening reactions relative to those in tempered martensite (Ref. 6).

The fracture mode in the multipass samples gives further evidence that these samples did not fail due to stress-relief cracking. The fracture surfaces of the HCM2S alloy showed extensive microvoid coalescence that is not typical of stress-relief cracking. Failure occurred along prior austenite grain and/or packet boundaries that are approximately normal to the tensile axis similar to a creep failure, but exhibited a large amount of plastic deformation. The 2.25Cr-1Mo multiple-pass samples are very similar to HCM2S. These samples also exhibited extensive plastic deformation and microvoid coalescence. Failure again occurred predominantly along grain boundaries that are approximately normal to the tensile axis.

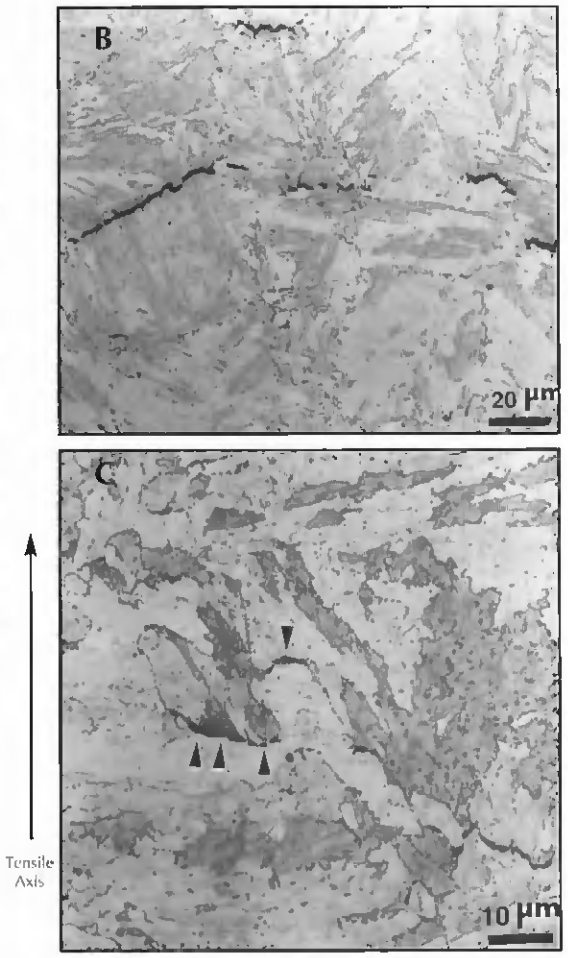

Fig. 9 — Photomicrographs of a cross section of a two-pass 2.25Cr-1Mo sample tested at 675°C.

Figure 10 is a schematic illustration of the microstructural changes that occur during the single-pass welding simulations and subsequent postweld heat treatment relative to the multiple-pass samples as well as the resultant failure mechanisms. In the single-pass samples, the alloying elements dissolve and austenite grains are allowed to grow uninhibited, leading to a large austenite grain size (although some carbides may remain undissolved as discussed above). During cooling, the austenite transforms to martensite and the alloying elements are trapped in solution. During PWHT, carbides precipitate both in the grain interiors (fine distribution) and at prior austenite grain boundaries (coarse). The grain boundary carbides could also be the result of incomplete dissolution during the first-pass thermal cycle. The grain boundary carbides deplete the adjacent region of alloying elements and a denuded zone forms. Elemental segregation may also occur. Any strain will be concentrated in soft denuded zones leading to low-ductility, intergranular failure with evidence of localized microvoid coalescence confined to the prior austenite grain boundary regions. It should be noted a denuded zone is not essential in order for stress-relief cracking to occur. In the case of the multiple-pass samples, the prior austenite grain and packet size are reduced during the second pass when a peak temperature of 925°C is utilized. This temperature is above the A_3 temperature into the single-phase austenite region. However, due to the fast heating and cooling rates, limited austenite grain growth occurred. Therefore, the second pass acted more as a tempering pass, allowing the carbides to form and/or coarsen. The carbides may have acted as nucleation sites for the microvoids. Carbide particles are well known to nucleate voids during both creep (Ref. 6) and conventional ductile failure (Refs. 7, 8). Small particles were frequently found within voids on the fracture surfaces of the alloys studied in this research. This was especially true of the HCM2S alloy as shown in Fig. 11 (particles indicated by arrows). The carbides formed during cooling after a simulated welding pass or during PWHT. Carbides that formed during cooling of the second pass have coarsened during the third pass and subsequent PWHT. The carbides present after the first pass, if any, were unresolvable at these magnifications and coarsened during subsequent passes and PWHT. The carbides, along with the lower peak temperature, may have contributed to producing a finer prior austenite grain size by pinning austenite grain boundaries. This would help to explain why there are many carbides located at prior austenite grain boundaries. In any event, the fine HAZ microstructure produced after the multipass simulations is much softer and is not expected to exhibit the strength gradients associated with a hard grain interior and soft denuded zone (which is expected in the single-pass simulations). As a result, the multipass specimens fail along grain boundaries and exhibit uniform plastic deformation, indicating that failure by a stress-relief cracking mechanism has been avoided.

Conclusions

The stress-relief cracking susceptibility of conventional 2.25Cr-1Mo and HCM2S steels was investigated using Gleeble techniques to simulate multiple-pass weld heat-affected zones. The results were compared to those from single-pass samples described in Part 1 of this paper (Ref. 1). The multipass samples of each material failed by microvoid coalescence and the times to failure increased in the multipass samples relative to the single-pass samples. The ductility increased with increasing PWHT temperature and both materials exhibited uniform plastic deformation. These features indicate the multipass simulations eliminated stress-relief cracking. Each

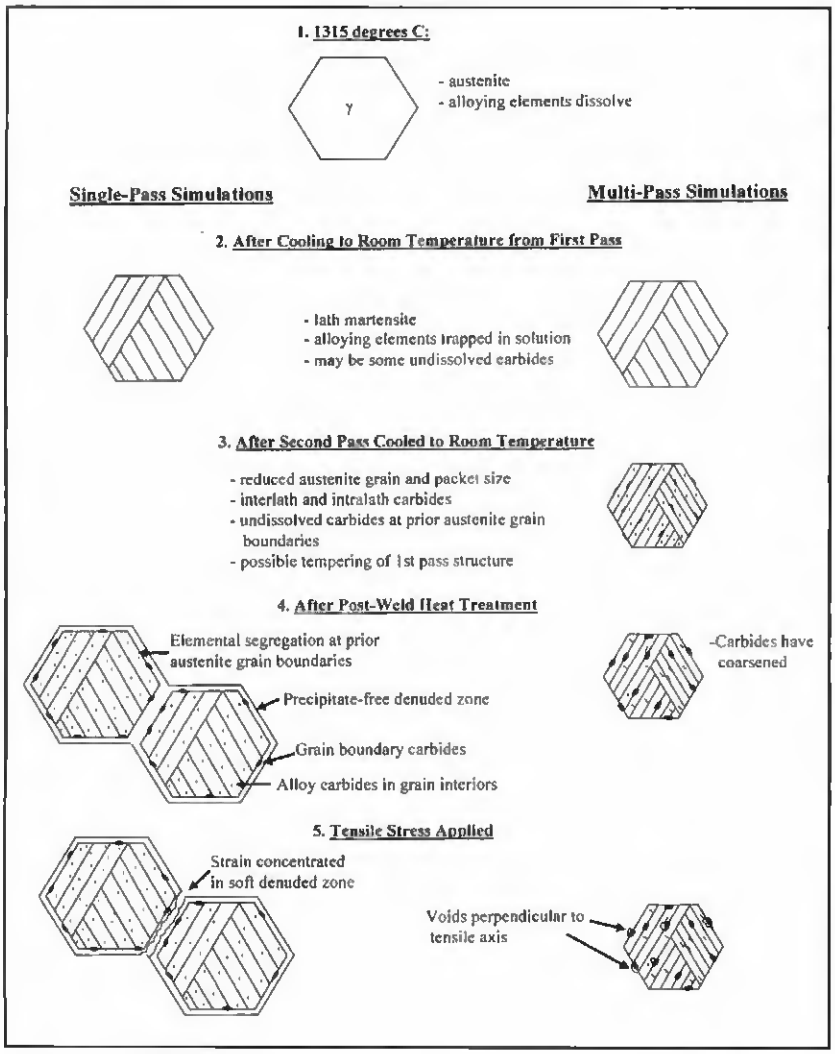

Fig. 10 — Schematic illustration of the microstructural changes and failure mode of single- and multiple-pass samples.

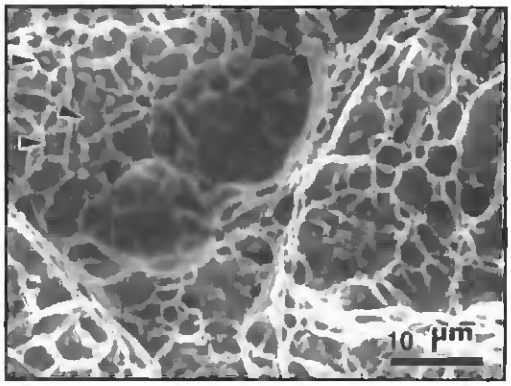

Fig. 11 — SEM photomicrograph of the fracture surface of a two-pass HCM2S sample tested at 675°C showing the presence of small particles within microvoids.

multipass sample failed primarily along grain boundaries that were located approximately normal to the tensile axis. The second pass, having a peak temperature of 925°C, resulted in a decreased packet and prior austenite grain size. Coarse carbides were present both along grain boundaries and within the grain interiors. These carbides formed during cooling from the first or second pass and coarsened during subsequent passes and/or PWHT. The carbides then acted as microvoid nucleation sites. The elimination of stress-relief cracking by the multipass simulations is attributed to formation of a HAZ microstructure which has uniformly softened and does not contain strength gradients associated with a hard grain interior and soft denuded zone.

Acknowledgments

The authors would like to gratefully acknowledge the sponsors of this research including Sumitomo Metal Corp., Mitsubishi Heavy Industries Ltd., Foster Wheeler Development Corp. and Pennsylvania Power and Light Co.

References

1. Nawrocki, J. G., DuPont, J. N., Robino, C. V., and Marder, A. R. 2000. The stress-relief cracking susceptibility of a new ferritic steel — part 1: single-pass heat-affected zone simulations. *Welding Journal* 79(12): 355-s.

2. Meitzner, C. F. 1975. WRC Bulletin 211, pp. 1–17.

3. *ASM Handbook* Vol. 6, Handbook of joining and brazing, ASM International, Materials Park, Ohio.

4. Nippes, E. F., Merrill, L. L., and Savage, W. F. 1949. Cooling rates in arc welds in ½-in. plates. *Welding Journal* 28(11): 556-s to 564-s.

5. Nippes, E. F., and Nelson, E. C. 1958. Predictions of weld heat-affected zone microstructures from continuous cooling transformation data. *Welding Journal* 37(7): 289-s to 294-s.

6. Kihara, S., Newkirk, J. B., Ohtomo, A., and Saiga, Y. 1980. *Metallurgical Transactions A*, 11A(6): 1019–1031.

7. Senior, B. A., Noble, F. W., and Eyre, B. L. 1986. *Acta Metallurgica* 34(7): 1321–1327.

8. Curry, D. A., and Pratt, P. L. 1979. *Materials Science and Engineering*, Vol. 37, pp. 223–235.

9. Baker, R. G., and Nutting, J. 1959. *Journal of the Iron and Steel Institute*, July, pp. 257–268.

10. Vinckier, A. G., and Pense, A. W., 1974. WRC Bulletin 197.

11. Lundin, C. D., Liu, P., Qiao, C. Y. P., Zhou, G., Khan, K. K., and Prager, M. 1996. WRC Bulletin 411.

12. Petch, N. J. 1953. *JISI*, Vol. 173, p. 25.

13. Hall, E. O. 1951. *Proc. Phys. Soc.* B, Vol. 64, p. 747.

14. Honeycombe, R. W. K., and Bhadeshia, H. K. D. H. 1996. *Steels: Microstructure and Properties*, 2nd ed., Halstead Press, New York, N.Y.